Journal of Materials Science and Chemical Engineering, 2020, 8, 1-22
https://www.scirp.org/journal/msce
ISSN Online: 2327-6053
ISSN Print: 2327-6045

Theoretical Analysis of a Shell and Tubes Condenser with R134a Working Refrigerant and Water-Based Oxide of Aluminum Nanofluid (Al_2O_3)

Élcio Nogueira

Department of Mechanical and Energy of State University of Rio de Janeiro, FAT/UERJ, Resende, Brazil
Email: elcionogueira@hotmail.com

How to cite this paper: Nogueira, É. (2020) Theoretical Analysis of a Shell and Tubes Condenser with R134a Working Refrigerant and Water-Based Oxide of Aluminum Nanofluid (Al_2O_3). *Journal of Materials Science and Chemical Engineering*, **8**, 1-22.
https://doi.org/10.4236/msce.2020.811001

Received: October 9, 2020
Accepted: November 10, 2020
Published: November 13, 2020

Abstract

The article analyzes a shell and tube type condenser's thermal performance using concepts of efficiency and effectiveness. Freon 134a is used as a coolant flowing through the shell. Water or water-based aluminum oxide nanoparticles are at relatively low saturation pressure in the tube. The condenser consists of 36 tubes divided into three central regions for analysis: superheated steam, saturated steam, and subcooled liquid. The three regions contain four tubes with three steps each, that is, 12 tubes. Region I, superheated steam, includes three horizontal baffles. Profiles of temperature, efficiency, and effectiveness are presented graphically for the three regions, with fixed refrigerant flow equal to 0.20 kg/s and fluid flow rate in the tube ranging from 0.05 kg/s to 0.40 kg/s. The experimental result for vapor pressure equal to 1.2 MPa and water flow equal to 0.41 kg/s was used as one of the references for the model's physical compatibility.

Keywords

Heat Exchanger, Condenser, Shell and Tubes, Freon 134a, Nanofluid

1. Introduction

Shell and tube heat exchangers are widely used in industrial processes. These heat exchangers are characterized by their versatility, applicability, and are still objects of study due to the countless possible physical arrangements that they allow. However, the deposition rate in media, shell, and tube can significantly affect the heat transfer rate, with a greater weight to the shell's side.

The article's objective is to analyze the thermal performance of a shell and tube type condenser using concepts of efficiency and effectiveness. Freon 134a is used as a coolant flowing through the shell. Water or water-based aluminum oxide nanoparticles are at relatively low saturation pressure in the tube. The condenser consists of 36 tubes divided into three central regions for analysis: superheated steam, saturated steam, and subcooled liquid. Region I, superheated steam, includes three horizontal baffles.

The length of the heat exchanger and the tube's diameter are, respectively, 0.762 m and 0.0127 m. The steam flow rate is fixed and equal to 0.20 kg/s, and the fluid flow rate in the tube varies from 0.05 kg/s to 0.40 kg/s. The steam enters at a temperature equal to 70.5˚C, and the fluid flows into the tube at a temperature equal to 25˚C. The tubes' configuration is of the square pitch type. Each Region consists of 12 tubes, with rows of 4 tubes and three passes in each Region. Region 1, superheated steam, uses three horizontal baffles for better heat exchange performance. The concepts of efficiency and effectiveness are used in each region for analysis of the thermal performance of the heat exchanger.

The article uses as a primary reference to the work carried out by Tzong-Shing and Jhen-Whei Mai [1], where a 48-tube condenser is analyzed using experimental resources and theoretical simulation, in a wide range of pressure and temperature, for heating water. The temperature difference between cold water at the inlet and hot water at the outlet of the condenser is, in most situations, high, on the order of 40˚C to 60˚C. Under such temperature differences, with high water outlet temperature, the condensing temperature increases, contributing to the rise in the refrigerant's sensitive heat rate by 25%. The authors' main objective was to analyze how to effectively recover sensitive heat and increase the shell and tube condenser's efficiency.

Ammar Ali Abd *et al.* [2] claim that pressure drop can be reduced by increasing the shell's diameter and the internal arrangements of the tubes, with the triangular pitch being the best option for increasing the overall heat exchange coefficient. Another desirable factor, which can improve thermal efficiency, is to reduce the number of baffles when possible.

Mohammad Reza Saffarian *et al.* [3] carry out a study to analyze the best option of the tubes' layout and shape in the heat transfer rate. They conclude that ellipsoidal tubes close to the shell wall, with an angle of attack equal to 90˚, and circular tubes in the center of the heat exchanger can increase heat exchange efficiency. However, ellipsoidal tubes with angles of attack equal to 90˚ produce maximum pressure drop.

Naveed ul Hasan Syed *et al.* [4] carry out an experimental study for analysis in a shell and tube type heat exchanger to verify the influence of the mass flow rates of the cold and hot fluids, water, on the global heat transfer coefficient. They conclude that an increase in flow rates increases the global heat transfer coefficient. However, an increase in the heat transfer rate of the cold fluid has a more significant influence. Also, an increase in hot water's inlet temperature positively

affects the overall heat transfer coefficient. Another factor positively affects heat exchange is the more significant turbulence caused by the flow. The authors implement a theoretical model for comparison with the results obtained experimentally but draw attention. In conclusion, this is not a generalization for shell and tube heat exchangers, despite the observed compatibility.

Rafał Laskowski *et al.* [5] argue that if suitable pipe diameter is implemented during the process of configuring a condenser, the greater thermal efficiency can be achieved, reflecting in the overall performance of the heat exchanger. Using a substantial diameter can lead to oversizing due to the larger heat exchange area and a higher cost for the heat exchanger. If the diameter is too small, it leads to more significant head loss and possibly lowers thermal efficiency. The authors propose an economical technique for optimally determining the diameter of a condenser. They use two methods to achieve the work's objectives: the method of minimizing entropy generation and the method of maximizing the output energy. The results obtained demonstrate that the first method is corroborated by the method of greater power. The diameter obtained is slightly larger than that obtained by the economical method, based on the condenser's costs. They draw attention to the fact that the results were determined based on the number of tubes and the condenser's length. Still, similar results can be obtained if the heat exchange area or constant pressure in the condenser is used, with a change in the number of tubes accordingly with the new parameters.

Élcio Nogueira [6] uses the concept of efficiency, efficacy, and irreversibility to obtain hot and cold fluid outlet temperatures in a shell and tube type heat exchanger, with nanofluid in the shell and hot water in the tube. He demonstrates that if the desired temperature is the lowest possible in the shell, it is not enough to have high efficiency if the heat exchange process's thermal effectiveness is low. High efficiency and high effectiveness are desirable for the cold fluid's highest possible outlet temperature, with high efficiency assuming greater relevance.

Nogueira, E. [7] uses the second law of thermodynamics for thermal analysis of a shell and tube type heat exchanger, with hot water flowing through the shell and a mixture of water-ethylene glycol with a fraction of nanoparticles in the tube. The flow regime is shown to have a significant effect on thermal performance. When the regime is laminar, with lower values for the number of Reynolds and greater relevance of the conductive effect caused by the nanoparticles, high effectiveness, and high irreversibility lead to lower temperatures in the shell. In these situations, the heat transfer rate approaches the maximum possible. Emphasizing that efficiency is high in all conditions analyzed.

Freon R134a has properties similar to CFC R-12 and has been used as the most appropriate alternative for the new environmental safety parameters. The work carried out by Ranendra Roy and Bijan Kumar Mandal [8] formulate thermodynamic properties for R134a using liquid density, saturation pressure, equation of state, and specific heat at constant volume. The authors draw attention to the fact that the developed formulations' properties are within acceptable limits for practical purposes.

2. Methodology

Figure 1 presents a simplified diagram for the condenser used for analysis. For convenience, the condenser was divided into three central regions: superheated steam, saturated steam, and subcooled liquid. The steam enters at a temperature equal to 70.5˚C, and the fluid flows into the tube at a temperature equal to 25˚C. Each Region consists of 12 tubes, with rows of 4 tubes and three passes in each Region. Region 1, superheated steam, uses three horizontal baffles for better heat exchange performance. The steam flow rate is fixed and equal to 0.20 kg/s, and the fluid flow rate in the tube varies from 0.05 kg/s to 0.40 kg/s. The properties of the fluids, for the temperature ranges considered, are shown in Table 1.

The input data for each of the regions are:

$$TREntr = 70.5^{\circ}C$$

$$TWEntr = 25.0^{\circ}C$$

$$Tsat = 46.02^{\circ}C$$

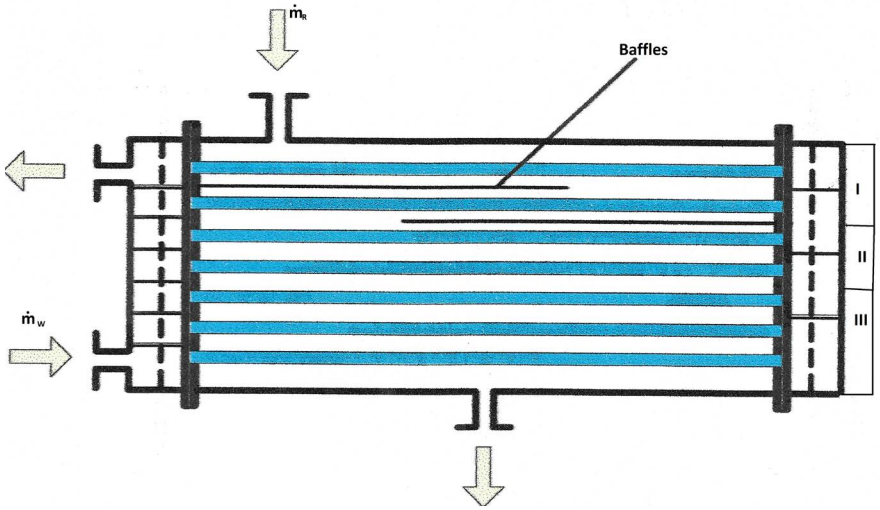

Figure 1. Simplified scheme of shell and tubes condenser (Adapted of Tzong-Shing Lee and Jhen-Whei Mai [1]).

Table 1. Properties of the fluids and nanoparticle used.

Properties	Freon R134a		Water	Al_2O_3
	I	III		
k W/(m·˚C)	15.447	74.716	0.60	31.922
Cp J/(kg·˚C)	1144.5	1498.4	4180	837.336
μ kg/(m·s)	12.373×10^{-6}	161.45×10^{-6}	0.758×10^{-3}	4.65×10^{-5}
P kg/m^3	50.085	1146.7	997	3950
ν N·m^2/s	2.47×10^{-7}	0.14×10^{-6}	0.8×10^{-7}	0.118×10^{-7}
α m^2/s	2.695×10^{-4}	4.35×10^{-5}	1.43×10^{-7}	9.65×10^{-6}
Pr	1091.1	310.7	5.68	818

$$NTube = 4 \tag{1}$$

$$Npass = 32 \tag{2}$$

$$D_W = 0.0127 \text{ m} \tag{3}$$

$$L = 0.762 \text{ m} \tag{4}$$

$$B = 0.0145 \text{ m} \tag{5}$$

$$CL = 1.0 \tag{6}$$

$$CTP = 0.85 \tag{7}$$

So, we have:

$$Pt = 1.25 D_W \tag{8}$$

$$De = \left(1.27/D_W\right)\left(Pt^2 - 0.785 {D_W}^2\right) \tag{9}$$

$$Dc = 3.0 D_W \tag{10}$$

$$PR = Pt/D_W \tag{11}$$

$$A_W = \pi D_W LNtubeNpass \tag{12}$$

$$Ds = 0.637\sqrt{CL/CTP}\sqrt{\left(ATPR^2 Dc\right)/L} \tag{13}$$

$$As = DsB\left(1.0 - D_W/Pt\right) \tag{14}$$

At where Pt is the tube pitch, De is the equivalent hydraulic diameter, D_W is the tube diameter, B is the baffles spacing, A_W is the heat exchange area on the side of the tubes, Ds is the shell diameter associated with each Region, As is the shell-side pass area.

$$Re_R = \left(\dot{m}_R De\right)/\left(As\mu_R\right) \tag{15}$$

$$Nu_R = 0.36 Re_R^{0.55} Pr_R^{1/3} \tag{16}$$

At where, $\dot{m}_R$ is the mass flow rate of the refrigerant, μ_R is the dynamic viscosity of the refrigerant, Re_R is the Reynolds number associate of the refrigerant, Pr_R is the Prandtl number of the refrigerant and Nu_R is the Nusselt number associate with the refrigerant.

$$h_R = \left(Nu_R k_R\right)/De \tag{17}$$

k_R is the thermal conductivity of the refrigerant and h_R is the convection heat transfer coefficient associated with refrigerant.

$$\rho_W = \phi\rho_{Al} + \left(1.0 - \phi\right)\rho_W \tag{18}$$

$$\mu_W = \mu_W * \left(1.0 + 2.5\phi\right) \tag{19}$$

$$\nu_W = \mu_W/\rho_W \tag{20}$$

$$Cp_W = \left(\phi\rho_{Al} Cp_{Al} + \left(1.0 - \phi\right)\rho_W Cp_W\right)/\rho_W \tag{21}$$

$$k_W = \left(K_{Al} + 2k_W + 2\left(k_{Al} - k_W\right)\left(1 + 0.1\right)^3 \phi\right)/\left(K_{Al} + 2k_W - \left(k_{Al} - k_W\right)\left(1 + 0.1\right)^2 \phi\right)k_W \tag{22}$$

$$\alpha_W = k_W/\left(\rho_W Cp_W\right) \tag{23}$$

$$Pr_W = \alpha_W/\nu_W \tag{24}$$

At where ρ_W is the density of the fluid in the tube, μ_W is the dynamic viscosity of the fluid in the tube, ν_W is the kinematic viscosity of the fluid in the tube, Cp_W is the specific heat of the fluid in the tube, k_W is the thermal conductivity of the fluid in the tube and Pr_W is the number of Prandtl associated with the fluid in the tube.

$$\dot{m}_{WT} = \dot{m}_W / N_{Tube} \tag{25}$$

$$Re_W = \left(4\dot{m}_{WT}\right)/\left(\pi D_W \mu_W\right) \tag{26}$$

At where $\dot{m}_W$ is the flow inlet of the fluid in the tubes, $\dot{m}_{WT}$ is the flow in each tube and Re_W is the Reynolds number associated with the flow in the tube.

$$Nu_W = 4.364 + \left(0.0722 Re_W Pr_W D_W\right)/L \quad \text{for } Re_W \le 2100 \tag{27}$$

$$Nu_W = \left(\left(ft/8\right)\left(Re_W - 10^3\right)Pr_W\right)\left(1+\left(D_W/L\right)\right)^{0.67} \Big/ \left(1+1.27\sqrt{\left(ft/8\right)}\left(Pr_W^{0.67}-1\right)\right) \tag{28}$$

$$\text{for } 2100 < Re_W \le 10^4$$

$$ft = \left(1.82\log\left(Re_W\right) - 1.64\right)^{-2} \tag{29}$$

$$Nu_w = 0.027 Re_w^{0.8} Pr_w^{1/3} \quad \text{for } Re_W > 10^4 \tag{30}$$

At where *ft* is the friction factor and Nu_W is the Nusselt number associate with the flow in the tube.

$$h_W = \left(Nu_W K_W\right)/D_W \tag{31}$$

$$Uo = 1/\left(1/h_R + 1/h_W\right) \tag{32}$$

At where U_O is the global heat transfer coefficient.

$$C_R = \dot{m}_R Cp_R \tag{33}$$

$$C_W = \dot{m}_W Cp_W \tag{34}$$

$$NTU = \left(A_W U_O\right)/Cmin \tag{35}$$

$$Fa = \left(NTU/2\right)\left(1 - C_*\right) \tag{36}$$

$$C_* = Cmin/Cmax \tag{37}$$

C_R is the thermal capacity of the refrigerant, C_W is the thermal capacity of the fluid in the tubes, *NTU* is called the Number of Thermal Units, *Cmin* is the smallest of the specific heats.

$$\sigma_T = Tanh\left(Fa\right)/Fa \tag{38}$$

$$\eta_T = 1/\left(1/\left(\sigma_T NTU\right) + \left(1+C_*\right)/2\right) \tag{39}$$

σ_T is thermal efficiency and η_T is the thermal effectiveness.

2.1. Solution Procedure for Region I

$$TW_i = T_{sat} - \Delta T_1 \tag{40}$$

ΔT_1 it is a value that makes it possible to determine the fluid inlet's actual temperature in Region I, for a given flow in the tube. It was determined by the difference between theoretical and experimental values. We used as reference the

experimental data from the second line of Table 1 of the reference [1]. An inlet temperature equal to 70.5˚C, inlet refrigerant pressure equal to 1.2 MPa, and mass flow rate for the tube's fluid equal to 0.41 Kg/s. Then, we define:

$$\Delta T_1 = 0.0 \text{ for theoretical results} \tag{41}$$

$$\Delta T_1 = 2.0 \text{ for the model with experimental results} \tag{42}$$

$$TR_i = TREntr \tag{43}$$

$$Q_{Actual} = \left(TR_i - TW_i\right) Cmin \Big/ \left(1/\left(\sigma_T NTU\right) + \left(1 + C_*\right)/2\right) \tag{44}$$

$$TW = \left(Q_{actual}/C_W\right) + TW_i \tag{45}$$

$$TR = TR_i - \left(Q_{Actual}/C_R\right) \tag{46}$$

At where, Q_{Actual} is the exchange of local heat between fluids, TW_i is the inlet temperature of the fluid flowing into the tube, TR_i is the fluid inlet temperature in the shell.

Do it:

$$TR_i = TR_i - \in_1 \tag{47}$$

Return to Equation (44) and recalculate Q_{Actual}, TW, TR.

$\in_1$ It is a value that allows greater precision in determining TR and TW.

The procedure at Region I ends when:

$$TR_i \le Tsat \tag{48}$$

when the exit condition of Region I is satisfied, we have the fluid's outlet temperature in the tube and inlet temperature for refrigerant, in Region II.

2.2. Solution Procedure for Region II

$$X = 1.0 \tag{49}$$

$$hlv = hv - hl \tag{50}$$

$$\mu_R = \mu_{Rl} X + \mu_{RV} \left(1.d0 - X\right) \tag{51}$$

$$\rho_R = \rho_{Rl} X + \rho_{RV} \left(1.d0 - X\right) \tag{52}$$

$$k_R = k_{Rl} X + k_{RV} \left(1.d0 - X\right) \tag{53}$$

$$Cp_R = Cp_{RL} X + Cp_{RV} \left(1.d0 - X\right) \tag{54}$$

$$Pr_R = Pr_{Rl} X + Pr_{RV} \left(1.d0 - X\right) \tag{55}$$

At where X is the steam fraction, the other terms are physical and thermodynamic properties in Region II.

$$Re_R = \left(\dot{m}_R De\right)/\left(As\mu_R\right) \tag{56}$$

$$\Delta_f = Tsat - T_{REf} \tag{57}$$

$$h_R = 0.943\left(\left(k_R \rho_R ghlv\right)/\left(\mu_R Ds\Delta_f\right)\right)^{0,25} \tag{58}$$

At where, Re_R is the number of Reynolds associated with the refrigerant in Region II, Δf is a reference temperature difference, h_R is the convection heat transfer coefficient, and $T_{REf} = 0$.

X varies from 1.0 to 0.0 in Region 2 and h_R varies with properties, which leads to different values for Uo, the global heat transfer coefficient. Thus, we have new calculations for efficiency and effectiveness. Heat exchange between fluids in Region II is achieved by:

$$\sigma_T = Tanh(Fa)/Fa \tag{59}$$

$$\eta_T = 1/\left(1/(\sigma_T NTU) + (1+C_*)/2\right) \tag{60}$$

$$Q_{Actual} = (Tsat - TW_i)Cmin/\left(1/(\sigma_T NTU) + (1+C_*)/2\right) \tag{61}$$

$$TW = TW_i - (Q_R/C_*) \tag{62}$$

Do it:

$$TW_i = TW_i - \in_2 \tag{63}$$

Return to Equation (60) and recalculate Q_{Actual}, TW.

$\in_2$ It is a value that allows greater precision in determining TW.

The procedure at Region II ends when:

$$X < 0.0 \tag{64}$$

when the exit condition of Region II is satisfied, we have the outlet and the inlet temperatures of the fluid in the tube, and inlet temperature for refrigerant, in Region III.

2.3. Solution Procedure for Region III

$$TW_i = 25^{\circ}\mathrm{C} \tag{65}$$

$$TR_i = Tsat \tag{66}$$

The initial calculations are identical to those of Region I, with a change in the refrigerant properties to Region III, as shown in Table 1. This means that Equations (15) to (17), Equations (33) to (39) must be recalculated.

$$Q_{Actual} = (TR_i - TW_i)Cmin/\left(1/(\sigma_T NTU) + (1+C_*)/2\right) \tag{67}$$

$$TW_o = TW - (Q_{Actual}/C_W) \tag{68}$$

$$TR_o = TR - (Q_{Actual}/C_R) \tag{69}$$

$$TW = TW_o \tag{70}$$

$$TR = TR - \Delta T_2 \tag{71}$$

Do it:

$$TW_i = TW_i - \in_2 \tag{72}$$

Return to Equation (67) and recalculate Q_{Actual}, TWo, TRo.

$\in_2$ It is a value that allows greater precision in determining TRo and TWo.

The procedure at Region III ends when:

$$TW_i \le TWEntr \tag{73}$$

when the exit condition of Region III is satisfied, we have the outlet temperature of the refrigerant.

ΔT_2 it is a value that makes it possible to determine the fluid inlet's actual temperature in Region I, for a given flow in the tube. It was determined by the difference between theoretical and experimental values. We used as reference the experimental data from the second line of Table 1 of the reference [1]. An inlet temperature equal to 70.5˚C, inlet refrigerant pressure equal to 1.2 MPa, and mass flow rate for the tube's fluid equal to 0.41 Kg/s. Then, we define:

$$\Delta T_2 = 0.0 \quad \text{for theoretical results} \tag{75}$$

$$\Delta T_2 = 0.085 \quad \text{for the model with experimental results} \tag{76}$$

Note: In Region I, the temperature varies with the refrigerant, since it knows its inlet and outlet temperatures. In Region III, the temperature in the tube varies with the temperature since the inlet and outlet temperatures are known.

3. Results and Discussion

3.1. Region I: Superheated Steam

Figure 2 shows the interpolation of experimental results obtained and presented in reference [1]. In this work, we use a pressure equal to 1.2 MPa to generate numerical and graphical results. For this pressure, the saturation temperature of R134a is equal to 46.02˚C, according to the results of interpolation performed and shown in Figure 3.

Figure 4 shows values for enthalpy of superheated steam associated with Region I. The enthalpy of R134a, in kJ/kg, can be obtained through the highlighted equation. The inlet pressure of the heat exchanger on the side of the shell is 1.2

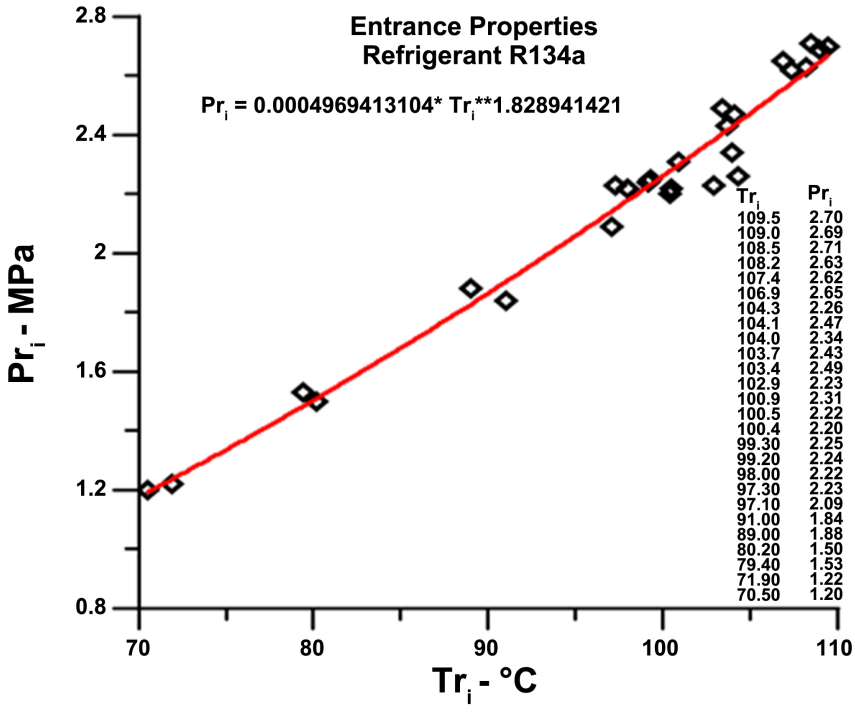

Figure 2. Inlet pressure as a function of inlet temperature according to experimental data presented in reference [1].

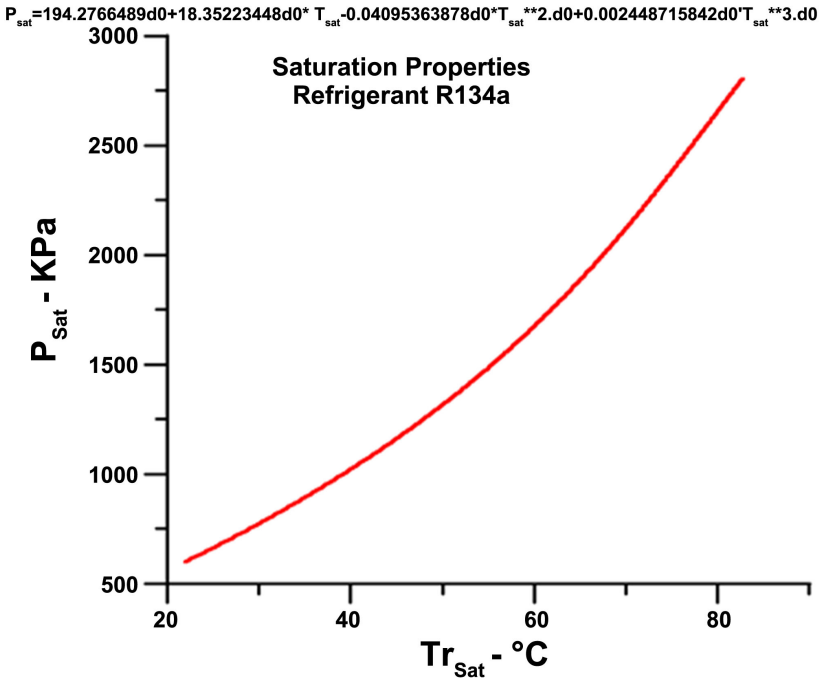

Figure 3. Saturation pressure as a function of the saturation temperature for R134a.

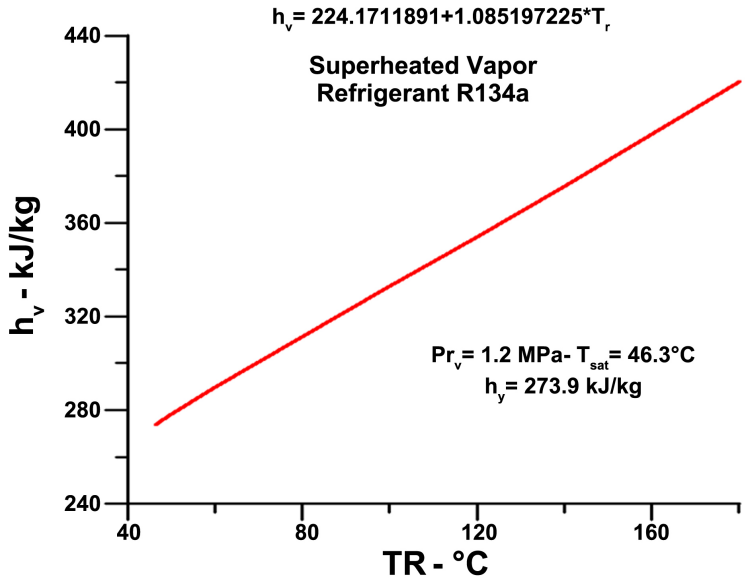

Figure 4. Enthalpy of superheated steam as a function of temperature for inlet pressure in the shell equal to 1.2 MPa.

MPa. The heat exchange with the water in the tubes depends on the steam's enthalpy and the mass flow rate of the steam, equal to 0.20 kg/s, in almost all situations analyzed in this work. The steam inlet temperature is 70.5˚C. The enthalpy saturation corresponds to 273.9 kJ/kg. The data used for interpolation for saturation temperature and enthalpy, highlighted in Figure 3 and Figure 4, were taken from references [8] [9] [10] [11].

Figure 5 shows the fluid temperature profiles in the shell and tubes, with a

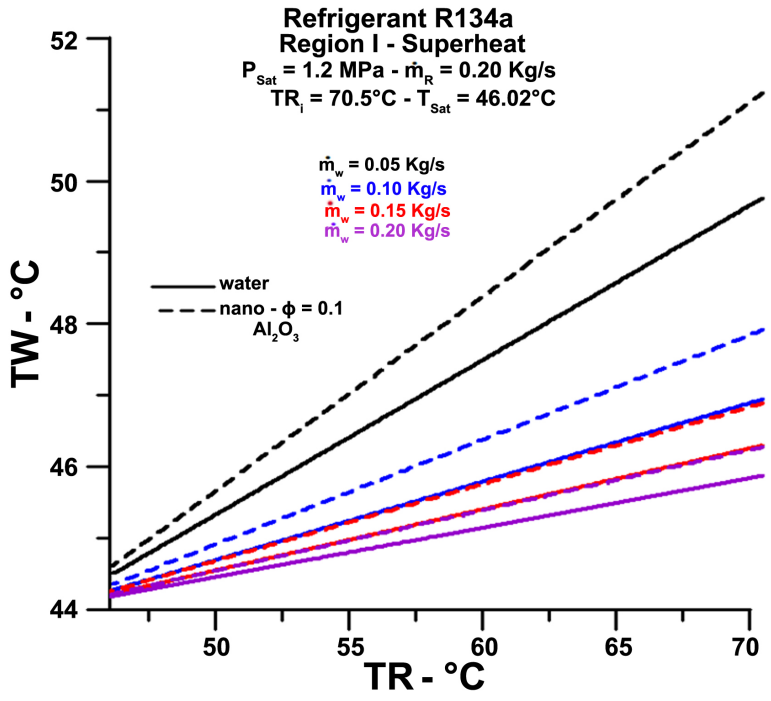

Figure 5. Temperature profiles for fluids in the tube (TW) and the shell (TR) in Region I.

relatively lower flow rate in the tube. Higher outlet temperatures for water and nanofluid are associated with lower mass flow rates in the tubes. Nanofuido has a higher outlet temperature compared to water. Also, the nanofluid temperature is slightly higher at the entrance to the Region I, for lower flow rates of the fluid in the tube.

Figure 6 shows the fluid temperature profiles in the shell and tubes for relatively hight mass flow rates in the tube. Higher outlet temperatures for water and nanofluid are associated with lower mass flow rates in the tubes. Nanofluid has a slighter higher outlet temperature compared to water. The fluid temperature at the tube entrance is not significantly different for the range of the considered mass flow rate in the tube.

Note that we have a fixed amount of energy to be donated by the steam in Region I since we have an inlet temperature of 70.5˚C and an outlet temperature of 46.02˚C. Another known quantity and defined a priori, imposed through experimental data, is the fluid inlet temperature in the tube in Region I. Thus, a more significant temperature difference between the outlet and the inlet for lower flow rates justifies the greater value of output for flow in the tube equal to 0.05 Kg/s. As nanofluid has thermal properties superior to water, like specific heat, the outlet temperature is higher for all flow rates analyzed.

The fluid inlet temperatures in the tube at Region I, for the entire mass flow range considered, are represented through Figure 7. These results are a graphical synthesis of the conclusions already presented in Figure 5 and Figure 6.

Table 2 presents numerical results for inlet and outlet temperatures, with the mass flow of the fluid covering laminar, transition, and turbulent regimes.

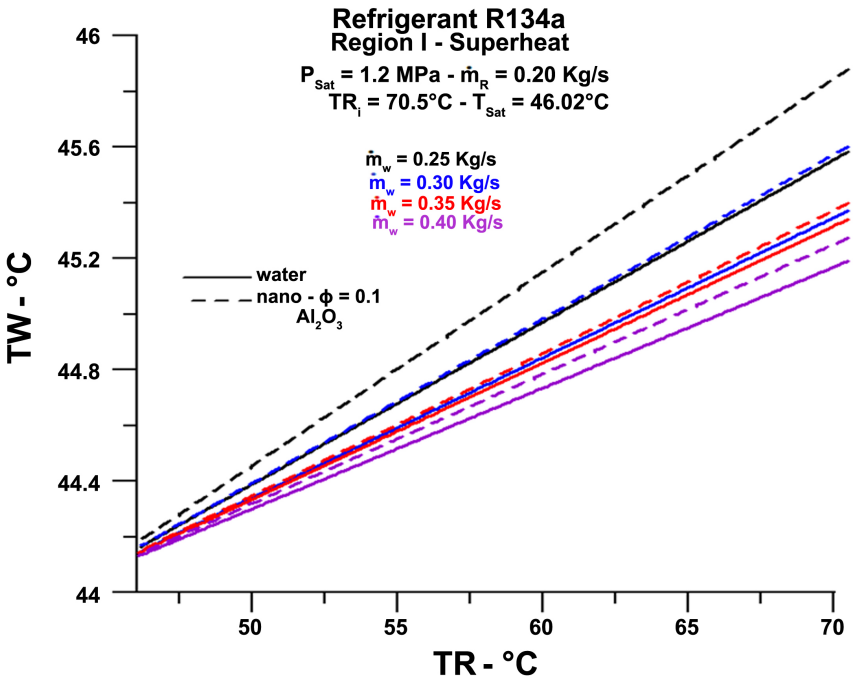

Figure 6. Temperature profiles for fluids in the tube (TW) and the shell (TR) in Region I.

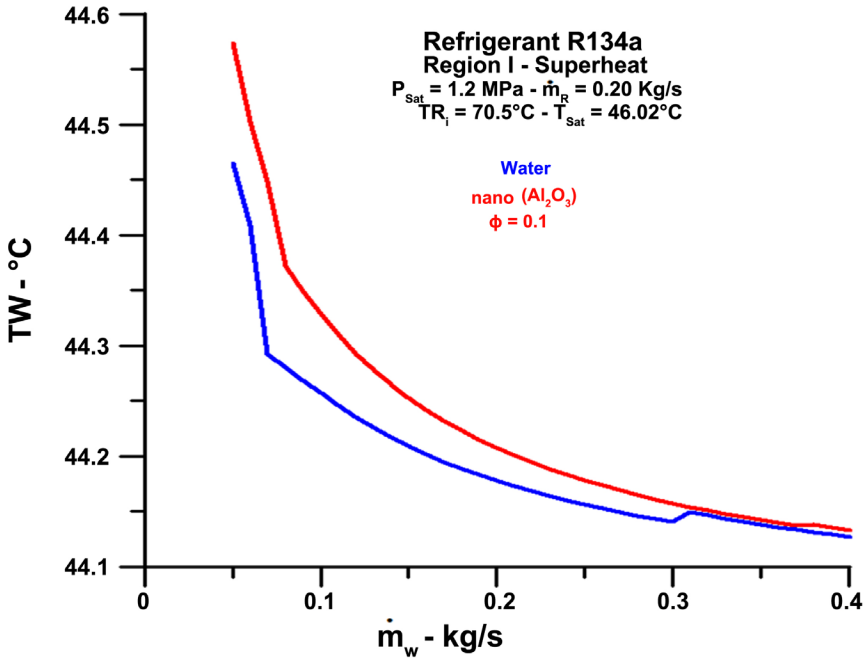

Figure 7. Inlet temperature of the fluid flowing into the tube in Region I.

Below, Table 2, we present a summary table of the temperatures obtained in Region I:

Figure 8 and Figure 9 show, respectively, the thermal efficiency and effectiveness for the heat exchange process throughout Region I. It is observed, initially, that efficiency is lower for nanofluid than pure water. In all cases, efficiency is too high, demonstrating that it is a process that works satisfactorily.

Table 2. Synthesis of some of the results obtained for Region I (Superheated).

REGIÃO I ($\dot{m}R$ = 0.20 kg/s)				
		Freon 134a	Pure Water	Nanofluid
Mass Flow rate 0.05 kg/s	Input pressure	1.2 MPa	1.2 MPa	1.2 MPa
	Input temperature	70.50˚C	44.46˚C	44.57˚C
	Output temperature	46.02˚C	49.76˚C	51.23˚C
Mass Flow rate 0.10 kg/s	Input pressure	1.2 MPa	1.2 MPa	1.2 MPa
	Input temperature	70.50˚C	44.25˚C	44.33˚C
	Output temperature	46.02˚C	46.95˚C	47.92˚C
Mass Flow rate 0.20 kg/s	Input pressure	1.2 MPa	1.2 MPa	1.2 MPa
	Input temperature	70.50˚C	44.18˚C	44.21˚C
	Output temperature	46.02˚C	45.87˚C	46.28˚C
Mass Flow rate 0.40 kg/s	Input pressure	1.2 MPa	1.2 MPa	1.2 MPa
	Input temperature	70.50˚C	44.14˚C	45.14˚C
	Output temperature	46.02˚C	45.19˚C	45.27˚C

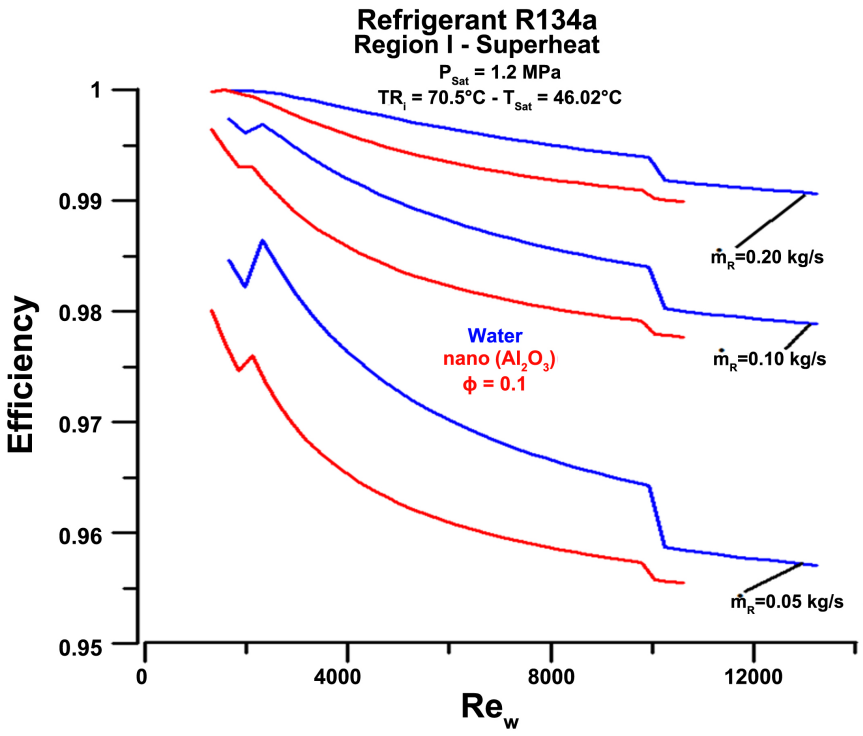

Figure 8. Thermal efficiency in Region I for different mass flow rates of R134a.

However, the effectiveness is very low for the mass flow rate of the refrigerant equal to 0.20 kg/s, demonstrating that there is a heat exchange much lower than the potential available; that is, the heat exchange is much lower than the maximum possible. For analysis, we vary the refrigerant flow rates in this single case, imposing slightly lower values. It can be seen that the effectiveness increases

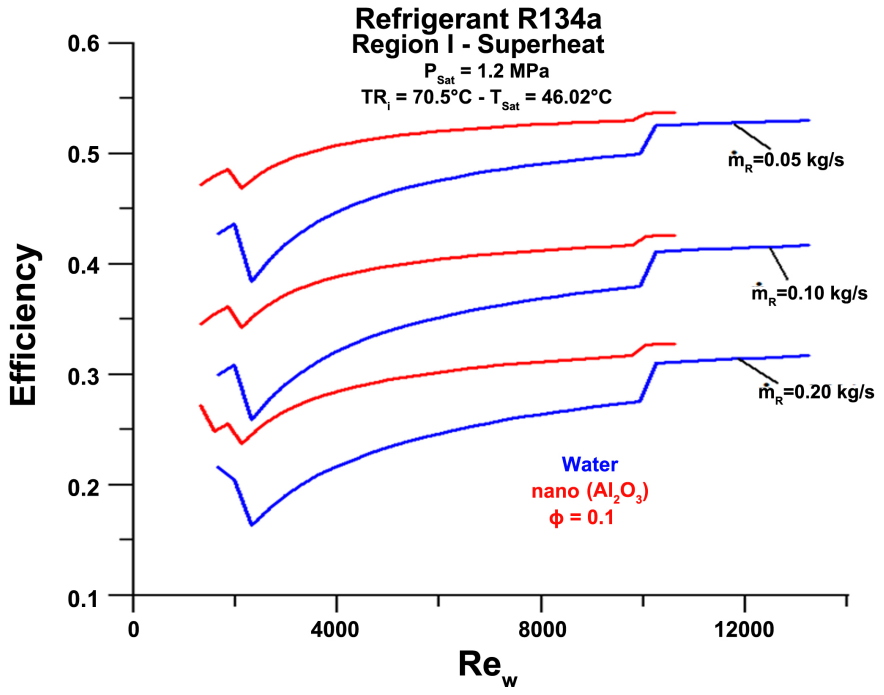

Figure 9. Thermal effectiveness in Region I for different mass flow rates of R134a.

with the decrease in the mass flow of the refrigerant, demonstrating that lower refrigerant flow rates allow greater heat exchange and that the heat transfer rate approaches the maximum possible.

All the previous results mentioned used $\Delta T_1 = 2.0^{\circ}\mathrm{C}$ which, in this case, is called a theoretical model with an experimental result taken from the reference [1]. The situation where $\Delta T_1 = 0.0$ is simply called a theoretical model.

Figure 10 shows the difference in temperature of the fluid inlet in the tube between the two models mentioned: theoretical and altered with the experimental result. For high flow in the tube, the difference tends to 2.0˚C, as expected, since this condition was imposed experimentally. However, for flow in the pipe equal to 0.05 kg/s, the difference drops to approximately 1.55˚C when draining water and becomes roughly equal to 1.45˚C when draining nanofluid.

3.2. Region II: Saturated Steam

Figure 11 presents the enthalpy associated with the subcooled liquid as a function of the saturation pressure. The equation that relates to the quantities in question is highlighted.

Figure 12 shows the temperature profile for the fluid in the tubes, depending on the vapor fraction. There is a significant increase between inlet and outlet temperature for different mass flow rates in the tubes.

It is observed that the outlet temperatures of the fluid in the tube, in Region II, are close for different values of the mass flow rate. The available energy comes from the steam and has the same value for each fraction of steam X. In this case, higher flows of liquid in the tube have smaller differences in temperature between

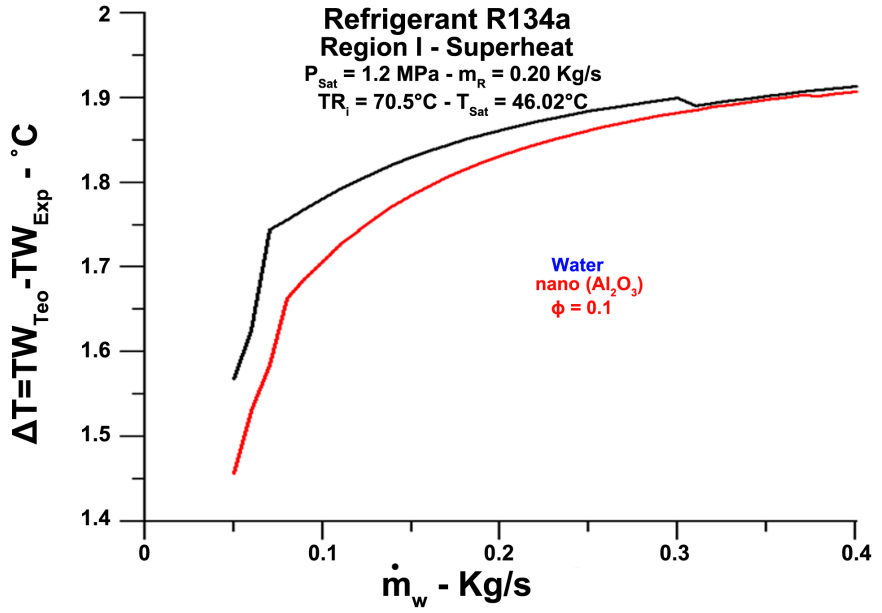

Figure 10. The actual difference between theoretical and experimental fluid inlet temperatures in Region I as a function of mass flow rate.

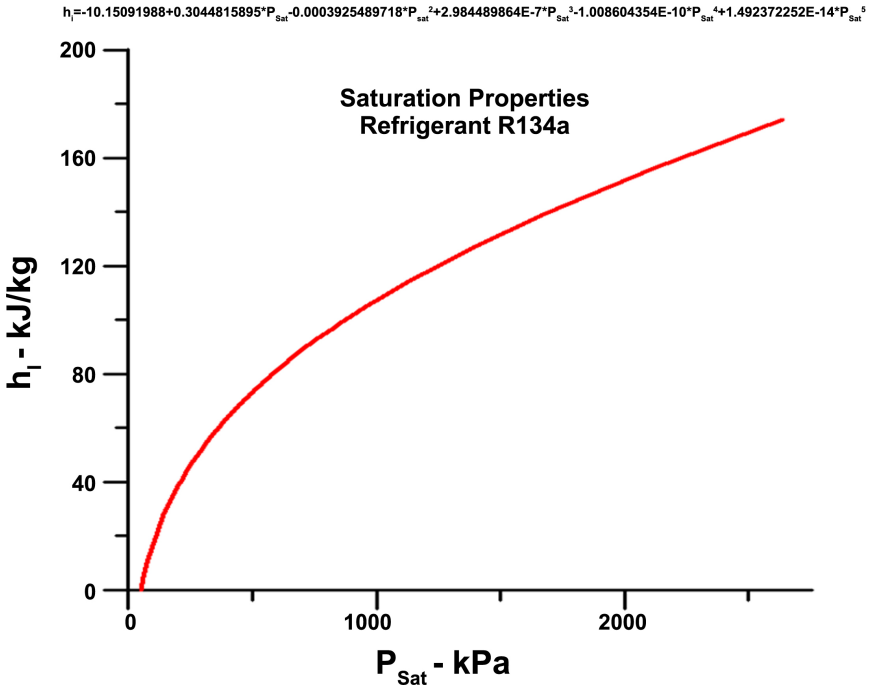

Figure 11. Enthalpy of R134a of the subcooled liquid as a function of saturation.

inlet and outlet. In contrast, lower flow rates, which absorb the same amount of energy, present a higher temperature difference between inlet and outlet. The nanofluid, which has more significant specific heat and thermal diffusivity, absorbs more energy. The temperature difference between the entry and exit of Region II is greater to water.

Figure 13 shows the fluid inlet temperatures in the tube, in Region II, for a

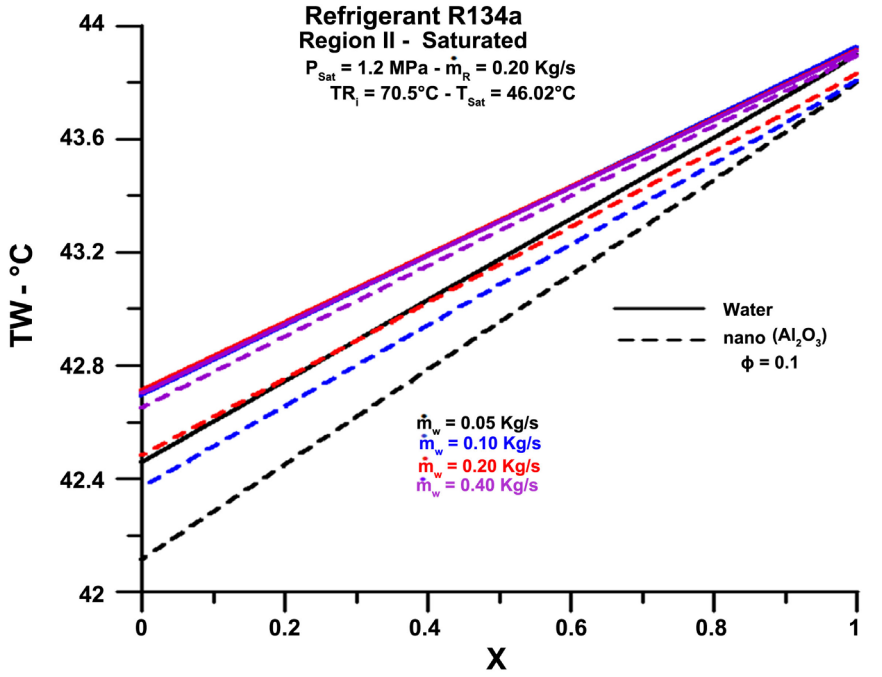

Figure 12. The fluid temperature in the tube as a function of the steam fraction in Region II.

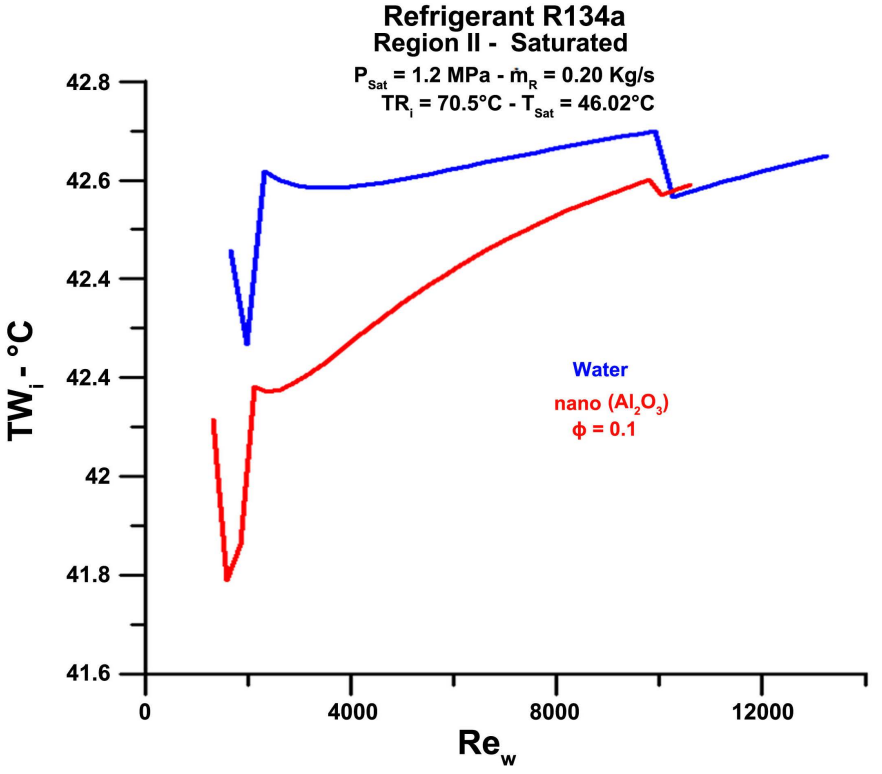

Figure 13. Inlet temperature of the fluid flowing into the tube in Region II.

wide range of Reynolds number. The results cover a laminar, transition, and turbulent regime.

3.3. Region III: Subcooled Liquid

Figure 14 shows temperature profiles for fluid in the tube and the shell in the Region of subcooled fluid, Region III. As already explained, the fluid inlet temperature in the tube is equal to 25˚C. The fluid's outlet temperature in the tube is higher for a higher flow rate with a slight elevation for the higher flow of nanofluid like is demonstrated by Figure 13. The refrigerant outlet temperatures decrease with the increase in the tube's mass flow, with slightly higher values for nanofluid. The refrigerant outlet temperature for mass flow in the tube stands out for mass flow rate equal to 0.40 kg/s, approximately equal to 39.0˚C (the numerically more accurate value is recorded in Table 3).

Table 3. Conditions and results obtained for Region III (Subcooled).

REGIÃO III ($\dot{m}R$ = 0.20 kg/s)				
		Freon 134a	Pure Water	Nanofluid
Mass Flow rate 0.05 kg/s	Input pressure	1.2 MPa	1.2 MPa	1.2 MPa
	Input temperature	46.02˚C	25.00˚C	25.00˚C
	Output temperature	45.19˚C 45.28˚C	42.46˚C	42.11˚C
Mass Flow rate 0.10 kg/s	Input pressure	1.2 MPa	1.2 MPa	1.2 MPa
	Input temperature	46.02˚C	25.00˚C	25.00˚C
	Output temperature	43.91˚C 44.43˚C	42.70˚C	42.37˚C
Mass Flow rate 0.20 kg/s	Input pressure	1.2 MPa	1.2 MPa	1.2 MPa
	Input temperature	46.02˚C	25.00˚C	25.00˚C
	Output temperature	42.30˚C 42.90˚C	42.71˚C	42.48˚C
Mass Flow rate 0.40 kg/s	Input pressure	1.2 MPa	1.2 MPa	1.2 MPa
	Input temperature	46.02˚C	25.00˚C	25.00˚C
	Output temperature	39.07˚C 39.84˚C	42.70˚C	42.65˚C

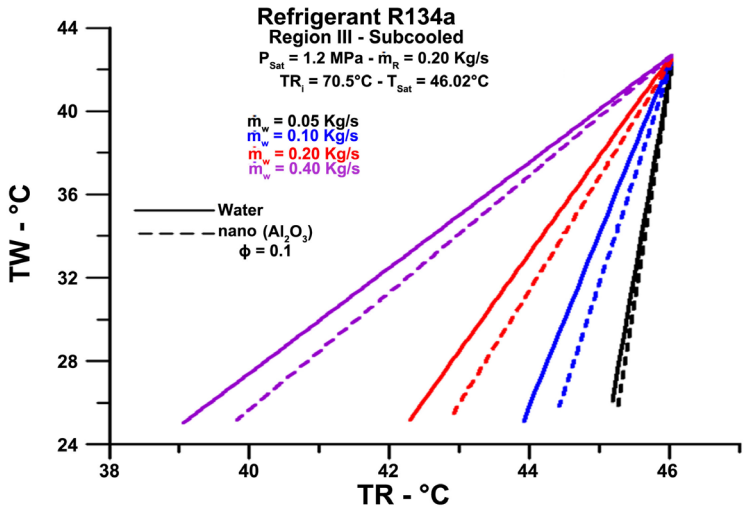

Figure 14. Temperature profiles for fluids in the tube (TW) and the shell (TR) in Region III.

The energy absorbed by the fluid in the tube is a function of its thermal capacity, which means that, if the inlet and outlet temperatures are practically the same for all flows, the one with the highest flow absorbs more energy. Greater energy absorption for higher flow rates leads to a lower outlet temperature for the refrigerant, as shown in Figure 14. Higher outlet temperatures of the refrigerant for nanofluid to water is justified by the lower outlet temperature of the fluid in the tube in Region III, as shown in Figure 13.

Figure 15 shows the fluid outlet temperatures in the refrigerant, in Region III, for a wide range of Reynolds number. The results cover a laminar, transition, and turbulent regime.

Figure 16 and Figure 17 presents, respectively, the thermal efficiency and effectiveness of the heat exchange process throughout Region III. It is observed that efficiency and effectiveness are lower for nanofluid than pure water. In all cases, efficiency is too high, demonstrating that it is a process that works satisfactorily. However, the effectiveness is very low for the mass flow rate of the refrigerant equal to 0.20 kg/s, demonstrating that there is a heat exchange much lower than the potential available; that is, the heat exchange is much lower than the maximum possible. Also, the effectiveness is lower than obtained at Region I, superheated steam Figure 9, which demonstrates that the heat exchange's potential with the refrigerant decreases along with the heat exchanger.

Table 3 presents numerical results for inlet and outlet temperatures, with the mass flow rate of the fluid covering laminar, transition, and turbulent regimes at Region III.

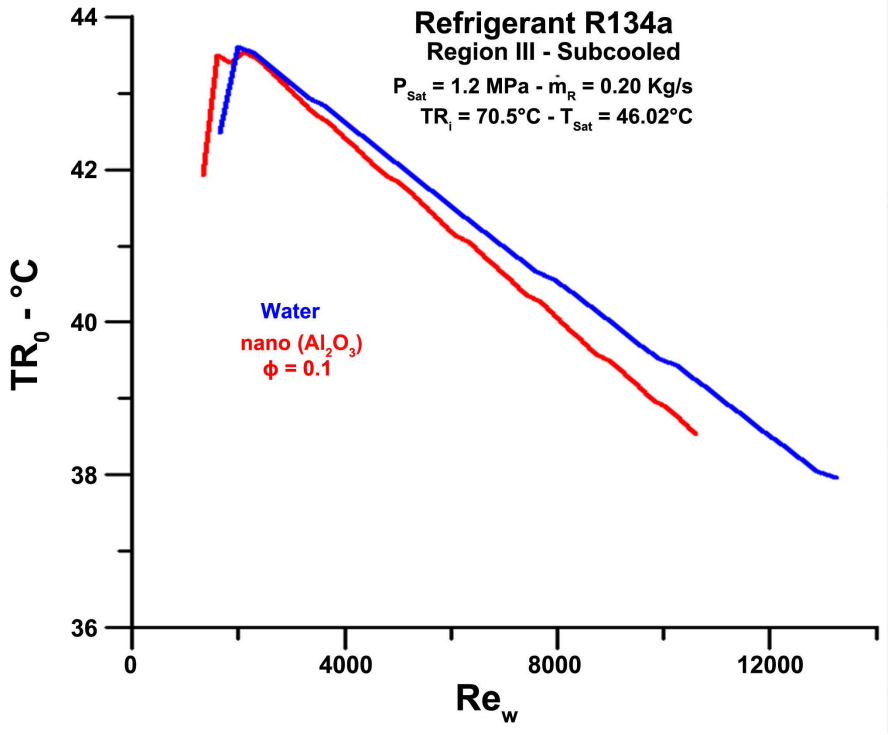

Figure 15. Outlet temperature of the refrigerant flowing into the tube in Region III.

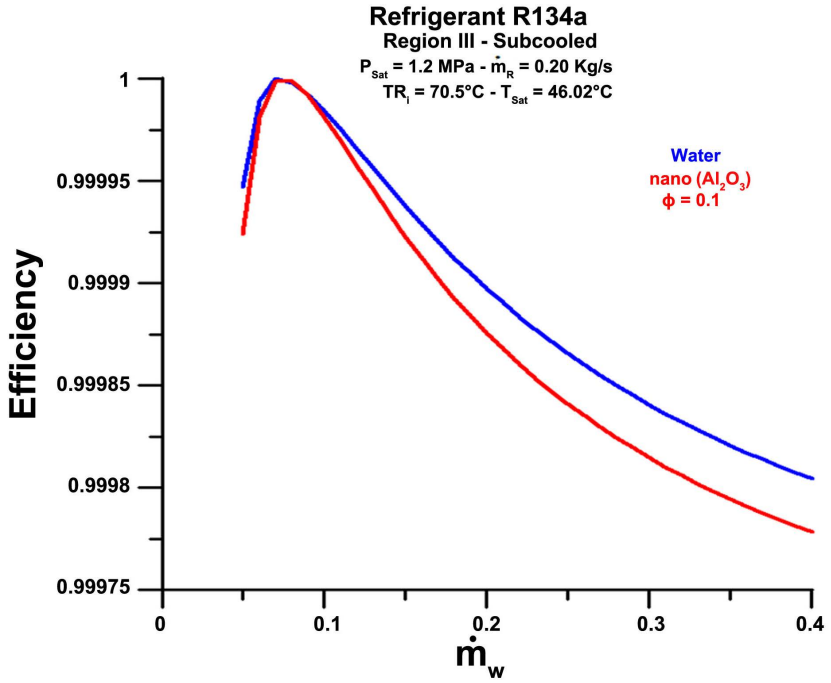

Figure 16. Thermal efficiency in Region III versus mass flow rate in the tube.

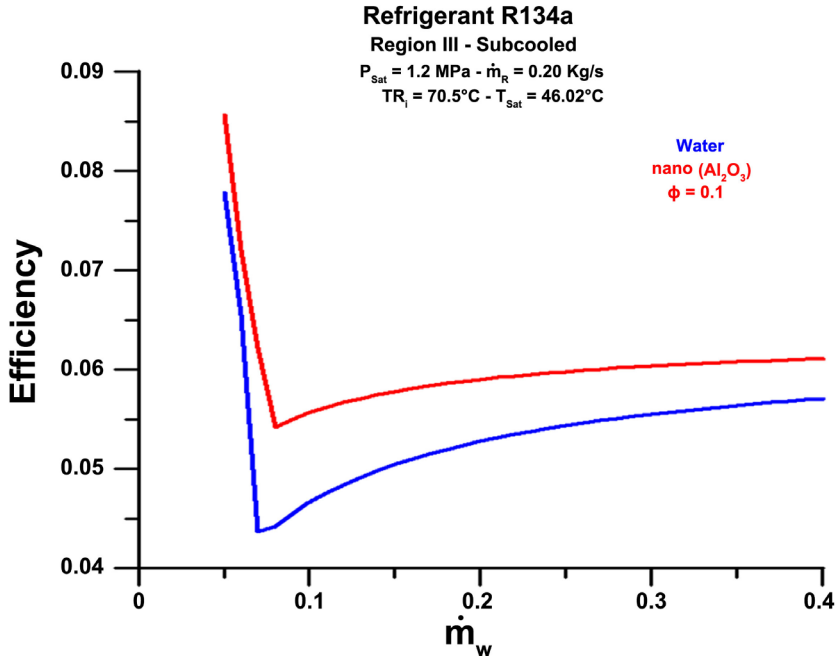

Figure 17. Thermal effectiveness in Region III versus mass flow rate in the tube.

Figure 18 shows the difference in temperature of the fluid inlet in the tube between the two models mentioned: theoretical and altered with the experimental result. For high flow in the tube, the difference is high in order of 7.0˚C. For flow in the pipe equal to 0.05 kg/s, the difference drops to approximately 1.0˚C.

Figure 19 shows a theoretical diagram for the water and coolant temperature profiles for each heat exchanger region.

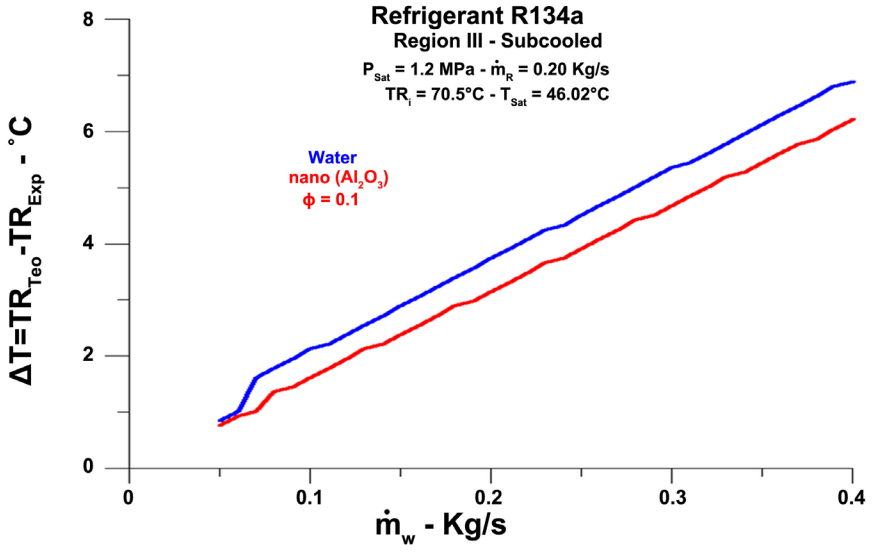

Figure 18. The actual difference between theoretical and experimental refrigerant outlet temperatures in Region III as a function of mass flow rate.

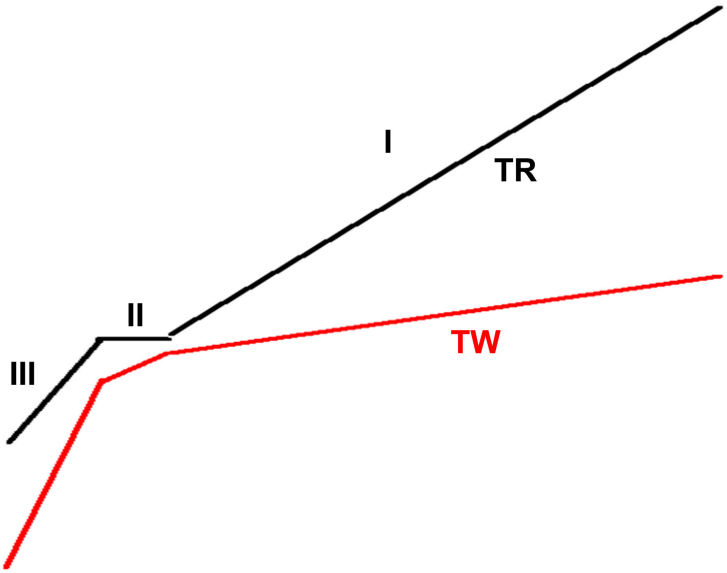

Figure 19. Theoretical temperature profiles for refrigerant R134a and fluid in the tube.

General observation to be emphasized, before presenting the conclusion, is that the theoretical and altered models for the experimental value approach for lower flow rates of the fluid in the tube. Note that, in this case, the calculated effectiveness value is relatively the highest in all situations analyzed. It is believed that it is possible to use it as a criterion for sizing the ideal condenser, one with high efficiency and high effectiveness.

4. Conclusions

The results presented demonstrate that the nanofluid has a thermal performance slightly superior to that of water, due to its more excellent thermal conductivity

and diffusivity, since its outlet temperature is higher than water.

Efficiency is high in all cases, with a negligible difference between fluids. However, the effectiveness is significantly higher for the nanofluid, which corroborates the fact that there is greater heat exchange with the refrigerant.

The most critical Region, concerning the highest temperature output in the tube, is Region I, saturated steam. The fluid's outlet temperature in the tube is higher for the lowest flow, *i.e.*, 0.05 Kg/s. In this case, the water leaves with a temperature close to 50˚C and the nanofluid with a temperature above one degree, that is, close to 51 ˚C.

The most critical region, concerning the refrigerant's lower temperature output, is Region III, subcooled liquid. The refrigerant outlet temperature is higher for the greatest flow, *i.e.*, 0.40 Kg/s. In this case, the 134a refrigerant leaves with a temperature close to 39˚C.

The most important parameter for measuring thermal performance, when efficiency is high, is effectiveness. A process that produces good thermal performance is an efficient one, works, and is effective.

There are two ways to improve thermal performance: maintaining the heat exchanger's physical configuration: decreasing the flow in the tube or decreasing the shell's flow. The latter case, seen through **Figure 9**, is the most relevant.

One of the hypotheses to be considered and analyzed in future works is that variations in the refrigerant inlet pressure, with higher working pressures, can increase the process's effectiveness, maintaining the same physical configuration as the heat exchanger. Another one is the increasing the number pass of tubes in each region. An increase in the exchange area, with a more significant number of tubes in each region, or an increase in the heat exchanger length, should enable better performance in the outlet temperatures.

Conflicts of Interest

The author declares no conflicts of interest regarding the publication of this paper.

References

[1] Lee, T.-S. and Mai, J.-W. (2011) Modeling and Simulation of the Heat Transfer Behavior of a Shell-and-Tube Condenser for a Moderately High-Temperature Heat Pump. In: Ahsan, A., Ed., *Two-Phase Flow, Phase Change and Numerical Modeling*, InTech, Department of Energy and Refrigerating Air-Conditioning Engineering, National Taipei University of Technology, Chinese Taipei.

[2] Abd, A.A., Kareem, M.Q. and Naji, S.Z. (2018) Performance Analysis of Shell and Tube Heat Exchanger: Parametric Study. *Case Studies in Thermal Engineering*, **12**, 563-568. https://doi.org/10.1016/j.csite.2018.07.009

[3] Saffarian, M.R., Fazelpour, F. and Sham, M. (2019) Numerical Study of Shell and Tube Heat Exchanger with Different Cross-Section Tubes and Combined Tubes. *International Journal of Energy and Environmental Engineering*, **10**, 33-46. https://doi.org/10.1007/s40095-019-0297-9

[4] Syed, N.H., Qurat-ul-Ain, Habib, M., Khan, N.A. and Ali, S. (2018) A Systematic

Study of the Influence of Process Variables on the Overall Heat Transfer Coefficient in a Shell and Tube Heat Exchanger. *Journal of Engineering and Applied Sciences*, **37**, 53-60.

[5] Laskowski, R., Smyk, A., Rusowicz, A. and Grzebielec, A. (2016) Determining the Optimum Inner Diameter of Condenser Tubes Based on Thermodynamic Objective Functions and an Economic Analysis. *Entropy*, **18**, 2-20. https://doi.org/10.3390/e18120444

[6] Nogueira, É. (2020) Efficiency and Effectiveness Concepts Applied in Shell and Tube Heat Exchanger Using Ethylene Glycol-Water Based Fluid in the Shell with Nanoparticles of Copper Oxide (CuO). *Journal of Materials Science and Chemical Engineering*, **8**, 1-12. https://doi.org/10.4236/msce.2020.88001

[7] Nogueira, E. (2020) Thermal Performance in Heat Exchangers by the Irreversibility, Effectiveness, and Efficiency Concepts Using Nanofluids. *Journal of Engineering Sciences*, **7**, F1-F7.

[8] Roy, R. and Mandal, B.K. (2014) Computer Based Thermodynamic Properties of Alternative Refrigerant R-134a. *Engineering Sciences International Research Journal*, **2**, 163-169.

[9] Oliveira, C.M.B.P. and Wakeham, W.A. (1999) Viscosity of R134a, R32, and R125 at Saturation. *International Journal of Thermophysics*, **20**, 365-373. https://doi.org/10.1023/A:1022640617694

[10] Shankland, I.R., Basu, R.S. and Wilson, D.P. (1988) Thermal Conductivity and Viscosity of a New Stratospherically Safe Refrigerant-1, 1, 1, 2-Tetrafluoroethane (R-134A). *International Refrigeration and Air Conditioning Conference*, Paper 41, 56-64.

[11] Huber, M.L. and McLinden, M.O. (1992) Thermodynamic Properties of R134a (1,1,1,2-Tetrafluoroethane). *International Refrigeration and Air Conditioning Conference*, Paper 184, 453-462.